Contribution from the Department of Chemistry,
The Ohio State University, Columbus, Ohio 43210

Metal–Metal Bonding in Dirhodium Tetracarboxylates. Structure of the Bis(pyridine) Adduct of Tetra-μ-acetato-dirhodium(II)

Y. B. KOH and G. G. CHRISTOPH*

Received March 23, 1978

The structure of the bis(pyridine) adduct of dirhodium tetraacetate has been analyzed by X-ray crystallographic techniques using three-dimensional diffractometer data. The rose red complex forms crystals with the monoclinic space group $C2/c$ (No. 15) and cell constants a = 9.923 (3) Å, b = 17.009 (6) Å, c = 12.539 (3) Å, and β = 106.60 (2)°. There are four formula units of the title complex per unit cell; the molecules reside on twofold symmetry axes, which are coaxial with the rhodium–rhodium vectors. The structure was solved by the heavy-atom Patterson method and refined by Fourier and least-squares techniques to conventional R factors of R_F = 0.031 and R_{wF}^2 = 0.048 for 2987 reflections. This compound appears to crystallize in several different forms; the one we have investigated is isostructural with that of the β (monoclinic) form of the bis(pyridine) adduct of tetra-μ-acetato-dicopper(II) and consists of molecules of the familiar dinuclear tetracarboxylate framework aligned parallel to the b axis. The Rh–Rh distance is 2.3963 (2) Å and the average of the two crystallographically independent Rh–N distances is 2.227 (2) Å. Within the error of measurement the dirhodium tetraacetate nucleus (excluding the hydrogen atoms) possesses exact D_{4h} symmetry. The molecule as a whole, however, has only C_2 symmetry, as the pyridine molecules are inclined to each other 59° and are rotated −26 and +33° from alignment with one of the acetate bridges. The Rh–Rh bond is 0.011 Å longer than in the structure of the diaquo adduct, consistent with the greater σ basicity of pyridine, which predicts a trans-influence lengthening of the Rh–Rh bond. The Rh–N bond is 0.1–0.2 Å longer than Rh–N(sp^2) bonds in mononuclear Rh(III) complexes; accordingly the trans influence of the Rh–Rh bond is very strong. Comparison with structural data for related dimolybdenum and dichromium tetracarboxylate complexes suggests that the Rh–Rh bond in these complexes is, surprisingly, intermediate in strength between the quadruply M–M bonded dimolybdenum(II) and dichromium(II) complexes, irrespective of whether it is assigned a formal bond order of 3 or 1. The long Rh–N distances and lack of preferred orientation of the pyridine rings relative to each other suggest that π back-bonding to the pyridine ligands groups, if present, is minimal.

Introduction

The small metal cluster complexes of the form $M_2(O_2CR)_4L_2$ (M = Cr(II), Mo(II), Rh(II), Cu(II), Re(III), Ru(III); L = axial ligands) have been the subject of extensive studies concerning the nature of the metal–metal bonds. Although the formal metal–metal bond order decreases from quadrupole for d^4–d^4 species (e.g., Mo(II), Re(III), Cr(II)) to nearly non-bonding for the d^9–d^9 configuration (e.g., Cu(II)),[1] there has been considerable controversy regarding the true picture of the bonding interactions between the metal atoms. In the dimeric rhodium(II) acetates, the question is whether the Rh–Rh bond is single or triple. The latter formulation was originally proposed by Cotton et al.,[2-5] primarily on the basis of bond length data, while the former is consistent with spectroscopic analyses[6] and, more recently, the results of SCF-Xα-SW calculations.[7]

In comparison with the strongly metal–metal bonded tetracarboxylate-bridged dimers, the dirhodium complex is unusual in that it is capable of forming stable diaxial adducts with a wide variety of ligands.[8-13] The sensitivity of the Rh–Rh bond distance to changes in the strength of the axial ligands should be a useful measure of the metal–metal interactions. We have accordingly prepared adducts $Rh_2(OAc)_4X_2$ with X = py, Et_2NH, CO, $P(OPh)_3$, $P(OMe)_3$, and PF_3 and are now examining their structures. We report here the results of the structure analysis of the bis(pyridine) complex and compare them with those reported for the diaquo adduct[2] as well as with the structural details for the analogous dimolybdenum and dichromium complexes.

Experimental Section

Preparation and Crystallization of $Rh_2(OAc)_4(py)_2$. $Rh_2(OAc)_4(CH_3OH)_2$ was prepared by a known procedure[14] from $RhCl_3 \cdot 3H_2O$ (Alfa Inorganics). Anhydrous methanol (Matheson Coleman and Bell) and pyridine (Fisher Scientific) were used as received, without further purification. The crystals of the bis(bipyridine) adduct were prepared by allowing pyridine vapor from a 4:1 mixture of anhydrous methanol and pyridine to slowly diffuse into a saturated methanol solution of $Rh_2(OAc)_4(CH_3OH)_2$. Most of the red crystals which formed in 1 week's time were monoclinic needles, although a small quantity of diamond-shaped and platelike crystals were also obtained. The adduct was stable at room temperature and essentially insoluble in hydrocarbon solvents, except for benzene and toluene in which it was slightly soluble. Upon heating, a slow ligand-exchange reaction was observed in oxygen-containing solvents: $Rh_2(OAc)_4(py)_2 + 2L \rightarrow Rh_2(OAc)RL_2 + 2py$, where L = MeOH, acetone, or THF. All manipulations were carried out at room temperature in an open atmosphere, although some efforts were made to exclude water vapor. IR (KBr pellet; Perkin-Elmer 457 grating IR spectrophotometer, range 4000–250 cm^{-1}): 3110 (w), 3073 (w), 3055 (w), 3008 (w), 2938 (w), 1590 (s), 1488 (m), 1450 (s), 1430 (s), 1351 (sh), 1349 (m), 1240 (w), 1230 (m), 1158 (w), 1082 (w), 1071 (m), 1047 (w), 1037 (m), 1013 (w), 1010 (w), 760 (m), 751 (m), 708 (s), 701 (s), 675 (sh), 630 (m), 594 (w), 433 (w), 428 (w), 385 (s), 336 (m). Vis–UV (neat pyridine; Cary 15; range 300–680 nm): λ_{max} 518 nm (ϵ 207 ± 15 M^{-1} cm^{-1}).

X-ray Data Collection. A small section of a needle-shaped crystal, 0.15 × 0.16 mm in cross section and 0.21 mm in length, was mounted on a goniometer approximately along the needle (001) axis. Precession photographs showed systematic absences for hkl of $h + k = 2n + 1$ and for $h0l$, $l = 2n + 1$, indicating as possible space groups either $C2/c$ or Cc. The unit cell constants were determined by a least-squares

Table I. Crystal Data for $Rh_2(OAc)_4(py)_2$ and $Cu_2(OAc)_4(py)_2$

	$Rh_2(OAc)_4(py)_2$	$Cu_2(OAc)_4(py)_2$[a]
a, Å	9.923 (3)	9.955 (5)
b, Å	17.009 (6)	17.314 (10)
c, Å	12.539 (3)	12.542 (10)
α, deg	90.0	90.0
β, deg	96.60 (2)	96.72 (10)
γ, deg	90.0	90.0
V, Å^3	2102 (1)	2144
space group	$C2/c$	$C2/c$[b]
Z	4	4
d(measd), g/cm^3	1.85 (1)	1.62 (1)
d(calcd), g/cm^3	1.896	1.615
T, °C	20 (1)	
μ(Mo Kα), cm^{-1}	15.8	

[a] Reference 39. [b] The original space group $A2/a$ given in ref 39 was changed to the standard symbol, and the cell constants were accordingly interchanged.

0020-1669/78/1317-2590$01.00/0

fit of the diffractometer setting angles for 15 carefully centered reflections for which $7.0° < 2\theta < 27.0°$ (Mo Kα). Relevant crystal data appear in Table I.

A total of 3558 intensities were measured for reflections with $4.0° < 2\theta < 60.0°$. Data were collected by the θ–2θ scan technique using graphite-monochromatized Mo Kα (λ 0.710 69 Å) radiation. The scan rate was varied from 2.0°/min for reflections giving less than 200 counts during a preliminary rapid intensity measurement to 12.0°/min for those giving more than 2000 counts. The scan width was 2.0° plus the width of the α_1–α_2 splitting. The background was measured at each end of each scan for a period of half the total scan time. The net scan counts were converted into integrated intensities using

$$I = R(C - T(B_1 + B_2))$$

where R is the scan rate, C is the scan count, B_1 and B_2 are the background counts, and T is the ratio of the scan time to the total background counting time. Seven standard reflections were remeasured after every 93 reflections in order to monitor the stability of the crystal and the machine. No sign of crystal decomposition, electronic malfunction of the equipment, or change in crystal alignment or orientation was observed throughout the course of data collection. Reflections (002), (110), (20$\bar{2}$), and (202) were not measured due to overflowed counting rates. The ψ scans of (004), (008), and (025), examined at 19° intervals in ψ, showed fluctuations of ±10% of their mean intensity values, primarily due to absorption effects. The indices of the crystal faces were determined from their diffraction angles to be (110), (1$\bar{1}$0), ($\bar{1}$10), ($\bar{1}\bar{1}$0), (001), and (00$\bar{1}$), and the crystal was measured optically with the aid of a Filar eyepiece. Absorption corrections were made by the method of Gaussian quadrature over a grid of 8 × 8 × 8 points. The resulting minimum and maximum transmission values were 0.771 and 0.857. Lorentz and polarization corrections were applied and the data placed on an absolute scale by means of a Wilson plot.[15] All reflections were assigned estimated standard errors using the formula

$$\sigma^2(I) = R(C + T^2(B_1 + B_2) + (pI)^2)$$

where $p = 0.02$ was chosen to account for the expected errors proportional to the diffracted intensity.[16] A total of 2987 unique data were obtained after the averaging of multiply measured and symmetry-related intensities and the deletion of systematically absent reflections. Of these, 2183 reflections had intensities greater than three standard deviations above the background. However, all 2987 reflections were used in all computations, on the grounds that to do otherwise introduces a small but unnecessary systematic bias into the data set.[17]

Solution and Refinement of the Structure. The structure was solved by the heavy-atom Patterson method; the rhodium atoms were assigned to independent positions on the crystallographic twofold axis on the assumption that the correct space group was $C2/c$ (this was confirmed by the successful completion of the refinement of the structure). The positions of the remaining nonhydrogen atoms were determined from Fourier and difference Fourier maps. Least-squares refinement of the coordinates and isotropic thermal parameters resulted in the agreement factors

$$R = \sum||kF_o| - |F_c||/\sum|kF_o| = 0.066$$

and

$$R_w = \left\{\frac{\sum(w^2(|kF_o|^2 - |F_c|^2)^2)}{\sum(w^2|kF_o|^4)}\right\}^{1/2} = 0.138$$

An attempt at this stage to locate hydrogen atoms was unsuccessful, and consequently the hydrogen atoms in the pyridine rings were fixed at the best theoretical positions at a distance of 0.95 Å from the trigonal-planar carbon atoms to which they were attached. With the hydrogen atoms in the methyl groups also held fixed, with a random orientation, the refinement was continued, including anisotropic temperature factors for the nonhydrogen atoms, until convergence was obtained at $R = 0.033$. Inspection of the low-angle reflections gave evidence of secondary extinction, and a parameter[18] to account for this was accordingly included in the refinement. Examination of the general planes of a difference Fourier map normal to the C–CH_3 axes now gave clues as to the correct location of the methyl hydrogen atoms, and these were now included at the derived positions. In the final cycles of least-squares refinement the parameters of all the hydrogen atoms were also allowed to vary. Convergence was assumed when the positional and thermal parameters showed virtually no shifts for the nonhydrogen atoms and shifts less than $^1/_{10}$ of the estimated standard deviations for the hydrogen atoms. The pyridine C(7)–H(7) distance (0.67 Å) as obtained in the last cycle of refinement was considered unrealistic and H(7) was assigned to a theoretical position on the twofold axis to give a more reasonable C–H distance of 0.95 Å. The maximum peak in the final difference Fourier map was 0.83 e/Å^3 and the minimum was −0.82 e/Å^3, not associated with any particular features in the structure. The general noise level of the map was ±0.30 e/Å^3. The final agreement factors were $R = 0.031$ and $R_w = 0.048$. The goodness of fit, $[\sum w(F_o^2 - F_c^2)^2/(n_o - n_p)]^{1/2}$, where $n_o = 2987$ observations and $n_p = 183$ variables, was 1.30. The final data-to-parameter ratio was 16.3:1. The function minimized in the full-matrix least-squares procedure was

$$\sum w(k^2F_o^2 - F_c^2)^2$$

where k is a scale factor and the weights $w = \sigma^{-2}(F_o^2)$. The scattering factors for O, N, and C were taken from ref 19a and that for Rh from ref 19b. The form factor of H was that of Stewart, Davidson, and Simpson.[20] The scattering factor of Rh was corrected for the real and imaginary components of anomalous dispersion using the values given in ref 19b.

All computations were done using the locally modified CRYM crystallographic computing system.[21] Table II contains the final values of all the refined parameters with their standard deviations estimated from the diagonal elements of the inverted matrix from the final least-squares cycle. The agreement between crystallographically distinct but chemically equivalent bonds indicates that the least-squares-derived esd's are perhaps underestimated 30%. The thermal vibration amplitudes are suggestive of small but significant rigid-body motions. Analysis of the temperature parameters with the program TLS[21b] proved most successful for a model consisting of three natural groupings, namely, the dirhodium tetraacetate nucleus and the two pyridine rings, with root-mean-square errors in the U_{ij} of 0.0030, 0.0029, and 0.0028 Å^2, respectively, compared with an error of 0.0043 Å^2 for the molecule as a whole rigid body. None of the librational amplitudes exceeded 2.8, 4.0, and 3.3° for the three groups. Bond distances corrected for these motions using the riding model are included in Table III (the angles were unaffected). No corrections exceeded 0.004 Å and most were 0.002 or 0.003 Å. Uncorrected distances will be used in comparisons with other structures (for which such corrections were not made). We point out that the correction to the Rh–Rh distance is some 15 times the esd derived for the uncorrected distance. The correction to the Rh–Rh bond length was, however, small and remarkably independent of the particular rigid librational model chosen, and we therefore feel comfortable in assigning to the corrected distance the esd shown in Table III. The listing of observed and calculated structure factor amplitudes and a table of nonbonded contacts are available.[22]

Results and Discussion

An ORTEP view of the molecule, giving the atom numbering convention, is shown in Figure 1. Tables III and IV summarize the bond lengths and bond angles. Least-squares planes calculated for representative sets of atoms and their mutual dihedral angles are set out in Table V.

The molecule possesses a (crystallographic) twofold axis that passes through the rhodium atoms. The dirhodium tetraacetate nucleus deviates only very slightly from D_{4h} point symmetry; chemically equivalent bonds and angles are all equal within the error of measurement, and the dihedral angles between the least-squares planes of the acetate bridges are less than $^1/_2\sigma$ from 90.0°. The Rh–Rh distance is short, 2.3963 (2) Å, and the Rh–N distance, at 2.227 Å, is more than 0.1 Å longer than in mononuclear Rh(III) complexes.[23]

Comparison of the structure of $Rh_2(OAc)_4(py)_2$ with that of $Rh_2(OAc)_4(H_2O)_2$,[2] for which the Rh–Rh distance is but 0.0108 Å shorter, shows essentially no differences in the tetraacetate frameworks; the average bond distances and angles in the respective structures are nearly identical: Rh–O 2.039 (2), 2.039 (8) Å; C–O 1.266 (3), 1.269 (4) Å; C–CH_3 1.499

Table II. Final Values of Least-Squares Refined Parameters for $Rh_2(OAc)_4(py)_2$[a,b]

atom	x	y	z	U_{11}	U_{22}	U_{33}	U_{12}	U_{13}	U_{23}
Rh(1)	0(0)	−5 574 (1)	25 000 (10)	221 (1)	138 (1)	202 (1)	0 (0)	33 (1)	0 (0)
Rh(2)	0 (0)	−19 663 (1)	25 000 (0)	212 (1)	139 (1)	186 (1)	0 (0)	33 (1)	0 (0)
O(1)	−14 048 (16)	−6 000 (8)	35 590 (12)	317 (8)	223 (8)	300 (8)	19 (6)	104 (7)	−13 (6)
O(2)	−15 068 (16)	−5 965 (8)	12 513 (12)	299 (8)	224 (8)	255 (7)	28 (6)	−26 (6)	0 (5)
O(3)	−13 561 (17)	−19 234 (8)	36 067 (12)	348 (9)	223 (8)	286 (8)	−12 (6)	132 (7)	2 (6)
O(4)	−15 670 (16)	−19 208 (8)	12 967 (12)	316 (8)	217 (7)	287 (8)	−9 (6)	−41 (7)	−28 (6)
C(1)	−17 755 (19)	−12 607 (14)	38 851 (14)	258 (9)	294 (9)	231 (8)	−15 (9)	51 (7)	−22 (9)
C(2)	−28 094 (28)	−12 503 (19)	46 668 (21)	416 (13)	409 (13)	399 (12)	11 (13)	207 (11)	6 (13)
C(3)	−19 832 (19)	−12 572 (13)	9 326 (14)	265 (9)	279 (9)	220 (8)	25 (9)	25 (7)	−13 (9)
C(4)	−31 520 (26)	−12 513 (19)	605 (20)	392 (12)	401 (13)	371 (11)	34 (13)	−123 (10)	−4 (13)
C(5)	−1 780 (27)	−88 451 (14)	33 891 (21)	475 (14)	278 (12)	422 (12)	3 (11)	42 (11)	−76 (10)
C(6)	−1 911 (40)	−80 364 (16)	34 193 (30)	779 (23)	303 (15)	650 (20)	40 (14)	50 (18)	−167 (13)
C(7)	0 (0)	−76 355 (25)	25 000 (0)	1027 (44)	134 (21)	889 (39)	0 (0)	−30 (33)	0 (0)
C(8)	−10 787 (21)	−36 774 (13)	27 472 (15)	275 (9)	274 (10)	268 (9)	−4 (9)	43 (7)	6 (8)
C(9)	−11 181 (29)	−44 875 (14)	27 553 (20)	458 (14)	279 (11)	362 (12)	−140 (10)	52 (11)	23 (9)
C(10)	0 (0)	−48 941 (20)	25 000 (0)	657 (26)	164 (17)	377 (18)	0 (0)	26 (18)	0 (0)
N(1)	0 (0)	−92 459 (15)	25 000 (0)	311 (15)	178 (13)	346 (15)	0 (0)	28 (12)	0 (0)
N(12)	0 (0)	−32 733 (14)	25 000 (0)	267 (13)	179 (12)	198 (11)	0 (0)	16 (10)	0 (0)

atom	x	y	z	B, Å²
H(21)	−263 (3)	−85 (2)	520 (3)	4.9 (0.8)
H(22)	−285 (3)	−173 (2)	503 (2)	4.4 (0.8)
H(23)	−356 (4)	−119 (2)	433 (3)	6.3 (1.0)
H(41)	−333 (4)	−173 (2)	−23 (3)	5.4 (0.8)
H(42)	−298 (3)	−87 (2)	−40 (3)	4.7 (0.8)
H(43)	−394 (4)	−112 (2)	39 (3)	5.3 (0.8)
H(5)	−36 (3)	−910 (2)	403 (2)	4.2 (0.7)
H(6)	−41 (3)	−780 (2)	401 (3)	4.6 (0.7)
H(7)	0 (0)	−708[c]	250 (0)	2.5 (0.9)
H(8)	−190 (3)	−339 (2)	285 (2)	3.5 (0.6)
H(9)	−187 (3)	−470 (2)	287 (2)	2.9 (0.6)
H(10)	0 (0)	−539 (3)	250 (0)	7.0 (1.5)

[a] Fractional coordinates have been multiplied by 10^5 (10^3 for hydrogen atoms) and the anisotropic thermal parameters by 10^4. The form of the temperature factor is $\exp\{-2\pi^2(U_{11}h^2a^{*2} + \ldots + 2klU_{23}b^*c^*)\}$. [b] g (secondary extinction parameter) = 0.5939 2 × 10^{-6}. See ref 18 for the form of the secondary extinction correction equation. [c] Calculated y coordinate based on the C–H distance of 0.95 Å. The final least-squares cycle gave −724 (3).

Table III. Bond Distances of $Rh_2(OAc)_4(py)_2$ with Estimated Standard Deviations

bond	distance, Å uncor	distance, Å cor	bond	distance, Å
Rh(1)-Rh(2)	2.3963 (2)	2.3994 (5)	C(2)-H(21)	0.95 (3)
Rh(1)-O(1)	2.035 (2)	2.038	C(2)-H(22)	0.93 (3)
Rh(1)-O(2)	2.038 (2)	2.041	C(2)-H(23)	0.82 (4)
Rh(2)-O(3)	2.042 (2)	2.046	C(4)-H(41)	0.89 (4)
Rh(2)-O(4)	2.040 (2)	2.043	C(4)-H(42)	0.91 (3)
Rh(1)-N(1)	2.231 (3)	2.234	C(4)-H(43)	0.96 (4)
Rh(2)-N(2)	2.223 (2)	2.225	C(5)-H(5)	0.95 (3)
O(1)-C(1)	1.265 (3)	1.266	C(6)-H(6)	0.88 (3)
O(2)-C(3)	1.266 (3)	1.267	C(7)-H(7)	0.95[a]
O(3)-C(1)	1.265 (3)	1.266	C(8)-H(8)	0.97 (3)
O(4)-C(3)	1.269 (3)	1.270	C(9)-H(9)	0.85 (3)
C(1)-C(2)	1.498 (4)	1.500	C(10)-H(10)	0.85 (6)
C(3)-C(4)	1.500 (3)	1.501		
C(5)-C(6)	1.376 (4)	1.377		
C(6)-C(7)	1.371 (4)	1.373		
C(8)-C(9)	1.379 (3)	1.380		
C(9)-C(10)	1.376 (3)	1.379		
N(1)-C(5)	1.336 (3)	1.338		
N(2)-C(8)	1.338 (3)	1.341		
O(1)···O(3)	2.252 (2)			
O(2)···O(4)	2.254 (2)			

[a] Theoretical value. The least-squares refinement gave 0.67 (4). The coordinates of H(7) were accordingly recalculated based on this distance.

(4), 1.498 (2) Å; Rh–Rh–O 87.98 (6), 88.1 (3)°; Rh–O–C 119.1 (1), 119.5 (3)°; O–C–CH_3 117.1 (2), 117.6 (6)°; O–Rh–O 89.72 (5), 91 (3)°; O–C–O 125.7 (1), 124.8 (3)°. The last pair of values is the only one where the members differ by more than one standard deviation from each other. It will be of interest in future structures in this series to see if, among

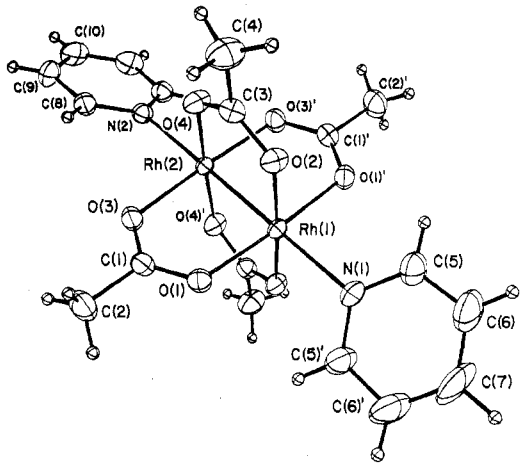

Figure 1. ORTEP[41] drawing of the molecule, showing the numbering scheme for the atoms. The thermal ellipsoids are drawn at the 50% probability level.

the geometric measures of the acetate bridges, the O–C–O angles are the more sensitive to changes in the rhodium–rhodium distance.

The value of the Rh–Rh–O angles in the above two structures reflect the fact that the rhodium atoms are very slightly displaced outward from the plane of the tetragonally disposed acetate oxygen atoms (0.072 Å in the bipyridine adduct). This should not be construed to imply that the rhodium atoms are restrained to their short internuclear separation (compared with ca. 2.69 Å expected for a single Rh–Rh bond)[24] by the acetate framework. As discussed below, a shorter rhodium–rhodium distance would be expected if the

Table IV. Bond Angles of $Rh_2(OAc)_4(py)_2$ with Estimated Standard Deviations (deg)

Rh(2)-Rh(1)-O(1)	87.96 (5)	C(8)-C(9)-C(10)	118.4 (3)
Rh(2)-Rh(1)-O(2)	88.13 (5)	C(9)-C(10)-C(9′)	119.7 (3)
Rh(1)-Rh(2)-O(3)	87.95 (4)	Rh(1)-N(1)-C(5)	120.7 (1)
Rh(1)-Rh(2)-O(4)	87.87 (4)	C(5)-N(1)-C(5′)	118.6 (3)
Rh(1)-Rh(2)-N(1)	180.00 (0)	Rh(2)-N(2)-C(8)	120.9 (1)
Rh(2)-Rh(1)-N(2)	180.00 (0)	C(8)-N(2)-C(8′)	118.2 (3)
O(1)-Rh(1)-N(1)	92.04 (7)	C(1)-C(2)-H(21)	112 (2)
O(2)-Rh(1)-N(1)	91.87 (7)	C(1)-C(2)-H(22)	112 (2)
O(1)-Rh(1)-O(2)	90.18 (7)	C(1)-C(2)-H(23)	108 (3)
O(1)-Rh(1)-O(2′)	89.69 (7)	C(3)-C(4)-H(41)	113 (2)
O(3)-Rh(2)-N(2)	92.05 (6)	C(3)-C(4)-H(42)	107 (2)
O(4)-Rh(2)-N(2)	92.17 (6)	C(3)-C(4)-H(43)	107 (2)
O(3)-Rh(2)-O(4)	89.74 (7)	N(1)-C(5)-H(5)	121 (2)
O(3)-Rh(2)-O(4′)	90.10 (7)	C(6)-C(5)-H(5)	116 (2)
Rh(1)-O(1)-C(1)	119.3 (1)	C(5)-C(6)-H(6)	119 (2)
Rh(1)-O(2)-C(3)	119.1 (1)	C(7)-C(6)-H(6)	123 (2)
Rh(2)-O(3)-C(1)	118.9 (1)	C(6)-C(7)-H(7)	120 (0.2)
Rh(2)-O(4)-C(3)	119.3 (1)	N(2)-C(8)-H(8)	119 (2)
O(1)-C(1)-C(2)	116.6 (2)	C(9)-C(8)-H(8)	118 (2)
O(3)-C(1)-C(2)	117.6 (2)	C(8)-C(9)-H(9)	116 (2)
O(2)-C(3)-C(4)	117.0 (2)	C(10)-C(9)-H(9)	125 (2)
O(4)-C(3)-C(4)	117.4 (2)	C(9)-C(10)-H(10)	120 (0.2)
O(1)-C(1)-O(3)	125.8 (2)	H(21)-C(2)-H(22)	107 (3)
O(2)-C(3)-O(4)	125.6 (2)	H(22)-C(2)-H(23)	106 (3)
N(1)-C(5)-C(6)	122.4 (3)	H(23)-C(2)-H(21)	110 (3)
C(5)-C(6)-C(7)	118.1 (3)	H(41)-C(4)-H(42)	116 (3)
C(5)-C(7)-C(6′)	120.4 (4)	H(42)-C(4)-H(43)	110 (3)
N(2)-C(8)-C(9)	122.6 (2)	H(43)-C(4)-H(41)	105 (3)

axial ligands were completely absent. We also note the recent report of a Rh–Rh separation of 2.316 (2) Å[25] in the structure of the *cation* $Rh_2(OAc)_4(H_2O)_2^+$ obtained by one-electron oxidation of the $Rh_2(OAc)_4(H_2O)_2$ system. The shortness of the Rh–Rh linkage may indeed depend upon the *presence* of the carboxylate ligands, in the sense that they facilitate metal–metal bonding interactions which might not otherwise exist,[26] but this is conceptually quite different from a constrictive restraint.

Our primary interest is in the nature of the Rh–Rh bond and in how it is affected by a change in the axial ligands. Qualitative trans-influence theory for a simple linear X–M–L system predicts that for increasing strength of the M–L σ bond the X–M bond should weaken and lengthen. The sensitivity of the M–X bond length to the M–L bond will depend upon the relative strengths of the bonds. Very strong M–X bonds should be less sensitive, and very weak M–X bonds more sensitive, to the nature of the ligand L. We have assembled in Table VI the metal–metal distances and related parameters for a variety of metal carboxylate dimers[26-29] for which L is H_2O or py or is absent. Since pyridine is a stronger base than water (respective pK_b's are 8.75 and 15.7), the expectation is that the M–py bond should be stronger than the M–OH_2 bond, and the M–M distance of the former should be longer due to the greater trans influence of py. If the ligand L is completely absent, the M–M bond should be shorter than with any L. The experimental results of Table VI amply bear this out. Unfortunately, two important structures, namely, $Mo_2(OAc)_4(H_2O)$ and $Rh_2(OAc)_4$ are missing, primarily because of difficulties of preparation. The fact that they are missing, however, does provide useful information on the relative strengths of the metal–metal bonds. Cotton et al.[3,30,31] attribute the difficulty in preparing diaxially substituted dimolybdenum complexes to the extremely strong quadrupole metal–metal bond, which itself exerts such a strong trans influence on the trans metal–ligand bond that it essentially weakens it out of existence. When stable adducts can be prepared, they possess extraordinarily long M–L bonds; e.g., the Mo–N bond in $Mo_2(O_2CCF_3)_4(py)_2$ is some 0.4 Å longer than a "normal" Mo–N bond. The Mo–Mo bond distance is also remarkably insensitive to the axial ligand type, further testament to its unusual strength.[31] By contrast, the quadruple M–M bond in the $Cr_2(OAc)_4L_2$ complexes is much more sensitive to the axial ligand (a change in Cr–Cr distance of about 0.12 Å in going from "no" ligand to pyridine, compared to an increase of only 0.04 Å for a similar change of L for Mo–Mo), and this is consistent with the inherent weakness of the Cr–Cr bond, despite the identical bond order of 4.[32] Thus the metal–metal bond distance alone is not a good indicator of bond order, although its *sensitivity* does seem to be a reasonable indicator of bond strength. The lack of the two key structures, $Mo_2(O_2CCF_3)_4(H_2O)_2$ and $Rh_2(OAc)_4$, prevents a direct

Table V. Least-Squares Planes and Dihedral Angles (deg) between Least-Squares Planes

Deviations (Å) from Planes[a]

	plane					plane	
atoms	A	B	C	D	atoms	E	F
Rh(1)	0.013	0.033	−0.070*	−0.075*	Rh(1)	0.000*	0.000*
Rh(2)	−0.023	−0.011			N(1)	0.000	
O(1)	−0.012		0.003		C(5)	0.003	
O(1)′			0.003		C(6)	−0.003	
O(2)		−0.040	−0.003		C(7)	0.000	0.000*
O(2)′			−0.003		C(6)′	0.003	
O(3)	−0.027			−0.002	C(5)′	−0.003	
O(3)′				−0.002	Rh(2)	0.000*	0.000*
O(4)		0.006		0.002	N(2)		0.000
O(4)′				0.002	C(8)		0.001
C(1)	0.005				C(9)		−0.001
C(2)	−0.011				C(10)	0.000*	0.000
C(3)		−0.012			C(9)′		0.001
C(4)		0.024			C(8)′		−0.001
dir cosines							
a	−0.6577	0.7403	0.0000	0.0000		−0.9634	−0.2677
b	−0.0150	−0.0181	1.0000	1.0000		0.0000	0.0000
c	0.6725	0.7527	0.0000	0.0000		0.1556	−0.9263

Dihedral Angles between Planes

planes	angle, deg	planes	angle, deg
A-B	91.1 (2.9)	A-F	25.6 (2.9)
A-E	33.3 (2.9)	B-F	63.3 (2.9)
B-E	57.8 (2.9)	E-F	58.9 (3.5)

[a] An asterisk indicates that an atom was given a weight of zero in the least-squares calculation.

Table VI. Selected Interatomic Distances (Å) and Angles (deg) for M_2(carboxylate)$_4L_2$ Compounds

complex	M-M	M-X	M-M-X	d(M-X) − d(M-O)	ref
$Mo_2(O_2CCF_3)_4$	2.090 (4)	2.72 (1)[a]	161.0 (4)[a]	0.66	27
$Mo_2(O_2CCF_3)_4(H_2O)_2$					
$Mo_2(O_2CCF_3)_4(py)_2$	2.129 (2)	2.548 (8)	171.0 (2)	0.43	28
$Cr_2(OAc)_4$	2.288 (2)	2.327 (4)[a]	164.6 (1)[a]	0.32	29
$Cr_2(OAc)_4(H_2O)_2$	2.362 (1)	2.272 (3)	175.6 (1)	0.25	2
$Cr_2(O_2CH)_4(py)_2$	2.408 (1)	2.308 (3)	179.3 (1)	0.29[c]	31
$Rh_2(OAc)_4$					
$Rh_2(OAc)_4(H_2O)_2$	2.3855 (5)	2.310 (3)	176.47 (6)	0.27	2
$Rh_2(OAc)_4(py)_2$	2.3963 (2)	2.227 (3)	180.00[b]	0.19	this work
$Rh_2(OAc)_4(Et_2NH)_2$[d]	2.403 (3)	2.308 (3)	176.2 (4)	0.27	33

[a] Distance and angle calculated to the atom of closest intermolecular contact, an acetate oxygen atom of a neighboring molecule. [b] Required by symmetry. [c] Note that the equatorial ligand is HCO_2^- instead of $CH_3CO_2^-$; these values are thus not directly comparable to others in this table. [d] Refinement in progress, $R = 0.10$, most atoms isotropic; the indicated errors are estimated from differences in chemically equivalent bonds.

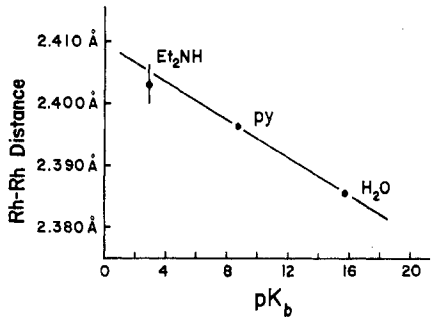

Figure 2. Plot of observed Rh–Rh distances as a function of ligand pK_b. The error bars are $\pm 1\sigma$; those for the H_2O and py adducts are smaller than the size of the dots.

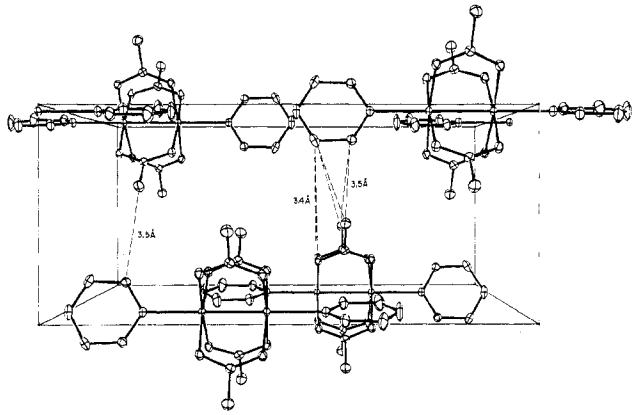

Figure 3. Packing diagram showing unit cell contents projected down the c axis. Thermal ellipsoids are shown at the 25% level; hydrogen atoms are omitted for clarity.

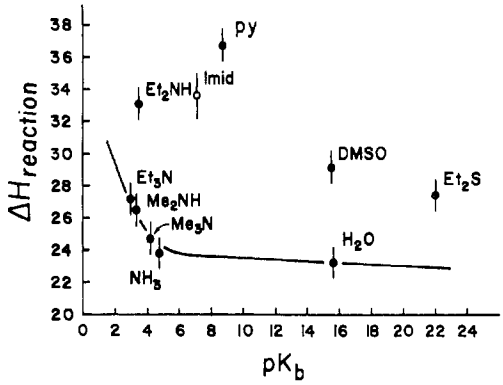

Figure 4. Plot of calorimetric ΔH's for the decomposition reaction $Rh_2(OAc)_4L_2(s) \rightarrow Rh_2(OAc)_4(s) + 2L(g)$ as a function of ligand pK_b. The point for imidazole (open circle) was estimated from solution spectrophotometric data (see text).

comparison of the response of the metal–metal bonds for these metals to changing axial ligand strength. (The reader will note that although we have included $Cr_2(O_2CH)_4(py)_2$ in this table, its bond parameters are actually not strictly comparable because of the replacement of bridging acetate by the weaker base formate.)

The short rhodium–rhodium distance and the fact that it increases only 0.011 Å when L = H_2O is replaced by L = py suggest to us that the Rh–Rh bond is intermediate in strength between that of the Mo–Mo and Cr–Cr bonds, irrespective of its bond order.

Qualitative trans-influence theory predicts that single and triple metal–metal bonds should respond somewhat differently to ligands which are π acceptors, and the question of possible π back-bonding to the pyridine ligand thus becomes important in assessing the π interactions between the metal atoms. Since the pK_b of a ligand is a measure of basicity toward a proton, it is presumably strictly a measure of the σ-donor properties of the ligand. In Figure 2 we have plotted the observed rhodium–rhodium distances for the diaquo and bis(pyridine) adducts and the preliminary[33] Rh–Rh distance for the bis(diethylamine) adduct against the pK_b's for these bases.

The essential linearity of this plot suggests that Rh–py π interactions are not significant in determining the length of the Rh–Rh bond; the change in the Rh–Rh distance can be explained completely by the differing σ-donor properties of the ligands. Because the M–N(py) distances in all of these dimers are longer than normal covalent M–N(sp^2) bond lengths,[23] we should expect that the relative magnitude of any $M_{d\pi}$–$N_{p\pi}$ interactions will be substantially weaker than normal simply as a consequence of the much reduced from normal $d\pi$–$p\pi$ overlap integrals.

This conclusion is supported by the lack of preferred orientation of the pyridine rings with respect to each other. One would expect that for strong metal–ligand π interactions that the pyridines would adopt an orthogonal orientation;[34] in the strongly metal–metal bonded systems, which also possess long metal–N distances, the pyridine ligands are in fact coplanar. In the $Rh_2(OAc)_4(py)_2$ complex the pyridine rings are inclined 59° to each other (Table V). The observed conformation of the pyridine rings appears to be due almost entirely to intermolecular packing forces, Figure 3. There are no intramolecular contacts of note[22] nor would there be for any orientation of the pyridine rings.

There is, however, some thermodynamic evidence for a Rh–ligand π interaction in complexes with pyridine or imidazole as the axial ligands. Kitchens and Bear have measured ΔH for the thermal decomposition

$$Rh_2(OAc)_4L_2(s) \rightarrow Rh_2(OAc)_4(s) + 2L(g) \qquad (1)$$

Table VII. Heats of Decomposition for the Reaction $Rh_2(OAc)_4I_2(s) \rightarrow Rh_2(OAc)_4(s) + 2L(g)$

L	ΔH, kcal/mol[a]	pK_b[b]	L	ΔH, kcal/mol[a]	pK_b[b]
NEt_3	27.2	2.98	imid	(33.6)[c]	7.05
$NHMe_2$	26.5	3.27	py	36.7 (37.8)[c]	8.75
$NHEt_2$	33.1	3.51	Me_2SO	29.1	15.54[d]
NMe_3	24.7	4.19	H_2O	23.2	15.7[e]
NH_3	23.8	4.75	SEt_2	27.4	20.99[d]

[a] Data from ref 35 unless otherwise noted. [b] "Handbook of Chemistry and Physics", R. C. Weast, Ed., 53rd ed, Chemical Rubber Publishing Co., Cleveland, Ohio, 1973. [c] Estimated from data given in ref. 11. [d] Calculated from data given in G. Perdoncin and G. Scorrano, *J. Am. Chem. Soc.*, 99, 6983–6986 (1977). [e] W. P. Jencks and J. Carriuolo, *ibid.*, 82, 1778–1786 (1960).

by differential scanning calorimetry,[35] and we reproduce their values in Table VII and plot them against pK_b in Figure 4. Excluding Et_2NH, a curve can be drawn through points for H_2O, NH_3, Me_2NH, Me_3N, and Et_3N (all σ donors), and the points for the potential π acceptors pyridine, imidazole, dimethyl sulfoxide, and diethyl sulfide all lie substantially above this curve. As the observed ΔH's are the sum of two factors, the bond dissociation energy and the energy of reorganization of the crystal as the structure is disrupted by the departing ligand, the scatter of the points may reflect the uncertain and structure dependent values of the latter contributor. It is of interest that a somewhat independent estimate of ΔH for reaction 1 with L = py can be obtained by combining the ΔH for the solution displacement reaction 2, measured

$$Rh_2(OAc)_4(py)_2(aq) + 2H_2O \rightarrow Rh(OAc)_4(H_2O)_2(aq) + 2py(aq) \quad (2)$$

spectrophotometrically[11] with the $\Delta H_{rxn(1)}$ for L = H_2O. This yields the value 37.8 kcal/mol, within the 1 kcal/mol error of measurement from that of $\Delta H_{rxn(1)}$ for L = py. A similar estimate for L = imidazole yields the additional point in Figure 4. Although the agreement lends a measure of reliability to the ΔH obtained by Kitchens and Bear, it does not remove the question of lattice energy contributions, nor does it explain why Et_2NH also lies far from the σ-donor curve. Although the agreement lends a measure of reliability to the ΔH values obtained by Kitchens and Bear, it does not remove the question of lattice energy contributions, nor does it explain why Et_2NH also lies far from the σ-donor curve.

Pyridine is at best a weak π-back-bonding ligand. Other evidence (e.g., ^{13}C NMR) is highly situation dependent and for Rh(III) complexes at least is somewhat contradictory.[36,37] Until more extensive and reliable data becomes available, the question of Rh–py π interaction in these complexes must remain unresolved.

After completion of our structure determination we were surprised to discover that the structure of the dirhodium complex described here is isostructural with that of the monoclinic form of the dicopper tetraacetate bipyridinate. (Two crystalline forms of the dicopper pyridine complex are known; the orthorhombic (α)[38] and monoclinic (β)[39] forms differ primarily in the rotational orientation of the pyridine molecules about the M–N bond.) Its cell constants are given in Table I for comparison; only the b axis length (the direction of the M–M vector) differs substantially between the two structures. Interestingly, the structures $M_2(OAc)_4(H_2O)_2$ for M = Cu(II), Cr(II), and Rh(II) are also all isostructural. Presumably the other crystal forms observed in the preparation of our dirhodium–bipyridine complex are isostructural with the orthorhombic bis(pyridine)–dicopper complex. An interesting possibility is that $Rh_2(OAc)_4(py)_2$ and $Cu_2(OAc)_4(py)_2$ may be induced to cocrystallize and form a continuous series of solid solutions.[40] This may be useful for study of the antiferromagnetic dicopper systems since the dirhodium complex is diamagnetic and could thus serve as an inert host matrix.

Acknowledgment. We are grateful to The Ohio State University Instruction and Research Computation Center for a generous grant of IBM/370 computer time.

Registry No. $Rh_2(OAc)_4(py)_2$, 13987-30-9.

Supplementary Material Available: Listings of the observed and calculated structure factor amplitudes and a table of nonbonded intra- and interatomic contacts less than 3.6 Å (32 pages). Ordering information is given on any current masthead page.

References and Notes

(1) F. A. Cotton, *Acc. Chem. Res.*, **2**, 240–247 (1969).
(2) F. A. Cotton, B. G. DeBoer, M. D. LaPrade, J. R. Pipal, and D. A. Ucko, *Acta Crystallogr., Sect. B*, **27**, 1664–1671 (1971).
(3) F. A. Cotton, *Chem. Soc. Rev.*, **4**, 27–53 (1975).
(4) M. J. Bennett, K. G. Caulton, and F. A. Cotton, *Inorg. Chem.*, **8**, 1–6 (1969).
(5) F. A. Cotton and J. G. Norman, Jr., *J. Am. Chem. Soc.*, **93**, 80–84 (1971).
(6) L. Dubicki and R. L. Martin, *Inorg. Chem.*, **9**, 673–675 (1970).
(7) J. G. Norman, Jr., and H. J. Kohlari, *J. Am. Chem. Soc.*, **100**, 791–799 (1978).
(8) L. A. Nazarova, I. I. Chernyaev, and A. S. Movozova, *Zh. Neorg. Khim.*, **10**, 539–540 (1965); **11**, 2583–2586 (1966).
(9) S. A. Johnson, H. R. Hunt, and H. M. Neumann, *Inorg. Chem.*, **2**, 960–962 (1963).
(10) T. A. Stephenson, S. M. Morehovse, A. R. Powell, J. P. Heffer, and G. Wilkinson, *J. Chem. Soc.*, 3632–3640 (1965).
(11) K. Das, E. L. Simmons, and J. L. Bear, *Inorg. Chem.*, **16**, 1268–1271 (1977).
(12) T. A. Mal'kova and V. N. Shafranskii, *Zh. Neorg. Khim.*, **19**, 2501–2505 (1974).
(13) G. Winkhaus and P. Ziegler, *Z. Anorg. Allg. Chem.*, **350**, 51–61 (1967).
(14) G. A. Rempel, P. Legzdins, H. Smith, and G. Wilkinson, *Inorg. Synth.*, **13**, 90–91 (1971).
(15) A. J. C. Wilson, *Nature (London)*, **150**, 151–152 (1942).
(16) W. R. Busing and H. A. Levy, *J. Chem. Phys.*, **26**, 563–568 (1957).
(17) F. Hirshfeld and D. Rabinovich, *Acta Crystallogr., Sect. A*, **29**, 510–513 (1973).
(18) A. C. Larson, *Acta Crystallogr.*, **23**, 664–665 (1967).
(19) "International Tables for X-Ray Crystallography", Kynoch Press, Birmingham, England: (a) Vol. III, 1962; (b) Vol. IV, 1974.
(20) R. F. Stewart, E. R. Davidson, and W. T. Simpson, *J. Chem. Phys.*, **42**, 3175–3187 (1965).
(21) (a) D. J. DuChamp, Paper B-14, American Crystallographic Association Meeting, Bozeman, Mont., 1965; (b) TLS: V. Schomaker and K. N. Trueblood, *Acta Crystallogr., Sect. B*, **24**, 63–76 (1968), modified for mass weighting of atoms a la R. F. Picone, M. T. Rogers, and M. Newman, *J. Chem. Phys.*, **61**, 4808–4813 (1974).
(22) Supplementary material.
(23) Some normal Rh(III)–N(sp^2) bond lengths are 2.09 (2) Å in $[RhCl_2(C_8H_{15}O)(\gamma\text{-pi})_2]_2$ (pic = picoline) (J. A. Evans, D. R. Russell, A. Bright, and B. L. Shaw, *Chem. Commun.*, 841–842 (1971)), 2.09 (2) Å in *trans*-$[Rh(py)_4Br_2](NO_3^-)(HNO_3)$ (G. C. Dobinson, R. Mason, and D. R. Russell, *Chem. Commun.*, 62–63 (1967)), 2.05 (1) Å in $Rh(Me_2SO)(py)_2Cl_3$ (P. Colamarino and P. Orioli, *J. Chem. Soc., Dalton Trans.*, 845–848 (1976)), and 2.12 (1) Å in $Rh(py)_2Cl_2$(*o*-di-*o*-tolylphosphino)benzyl) (R. Mason and A. O. C. Towl, *J. Chem. Soc. A*, 1601–1613 (1970)).
(24) K. G. Caulton and F. A. Cotton, *J. Am. Chem. Soc.*, **93**, 1914–1918 (1971).
(25) J. J. Ziolkowski, M. Moszner, and T. Glowiak, *J. Chem. Soc., Chem. Commun.*, 760–761 (1977).
(26) J. G. Norman, Jr., H. J. Kohlari, H. B. Gray, and W. C. Trogler, *Inorg. Chem.*, **16**, 987–993 (1977).
(27) F. A. Cotton and J. G. Norman, Jr., *J. Coord. Chem.*, **1**, 161–172 (1971).
(28) F. A. Cotton and J. G. Norman, Jr., *J. Am. Chem. Soc.*, **94**, 5697–5702 (1972).
(29) F. A. Cotton, C. E. Rice, and G. W. Rice, *J. Am. Chem. Soc.*, **99**, 4704–4707 (1977).
(30) D. M. Collins, F. A. Cotton, and C. A. Murillo, *Inorg. Chem.*, **15**, 1861–1866 (1976).
(31) F. A. Cotton, M. Extine, and L. D. Gage, *Inorg. Chem.*, **17**, 172–176 (1978).
(32) M. Benard and V. Veillard, *Nouv. J. Chim.*, **1**, 97–99 (1977).
(33) Y. B. Koh and G. G. Christoph, to be submitted.
(34) The high axial symmetry of the $Rh_2(OAc)_4$ complex framework enforces the degeneracy of the d_{xz} and d_{yz} orbitals. We thus can construct equivalent linear combinations of the form $d_{az} = (\sin\alpha)d_{xz} + (\cos\alpha)d_{yz}$ and $d_{bz} = (\sin\alpha)d_{xz} - (\cos\alpha)d_{yz}$, where α is the angle of rotation about the Rh–Rh axis. Thus a preferred orientation of the pyridine ligands relative to the acetate linkages should not be expected and is not observed; the appropriate

dihedral angles in $Rh_2(OAc)_4py$, β-$Cu_2(OAc)_4(py)_2$, α-$Cu_2(OAc)_4(py)_2$, $Cr(O_2CH)_4(py)_2$, and $Mo_2(O_2CCF_3)_4(py)_2$ are +33 and −26°, +33 and −26°, 30°, 30°, and 0°. However, if a pyridine ligand does have π interactions with the metal d_{az} or d_{bz} orbitals, the symmetry is immediately reduced from C_4 to C_2 and the d_{az} and d_{bz} orbitals are no longer degenerate, and this is communicated through the metal–metal bonding region to the opposite side. As the second pyridine π^* orbital will interact most effectively with the metal d_{az} or d_{bz} orbital nearest to it in energy, it should assume an orientation orthogonal to that of the first pyridine ring—one py will utilize the d_{az} of metal atom 1 and the other the d_{bz} of metal atom 2.

(35) J. Kitchen and J. L. Bear, *J. Inorg. Nucl. Chem.*, **31**, 2415–2421 (1969).
(36) D. K. Lavallee, M. D. Baughman, and M. P. Phillips, *J. Am. Chem. Soc.*, **99**, 718–724 (1977).
(37) R. D. Foust and P. C. Ford, *J. Am. Chem. Soc.*, **94**, 5686–5696 (1972).
(38) F. Hanic, D. Stempelova, and K. Hanicova, *Acta Crystallogr.*, **17**, 633–639 (1964).
(39) G. A. Barclay and C. H. L. Kennard, *J. Chem. Soc.*, 5244–5251 (1961).
(40) Conditions for formation of solid solutions are described in "Molecular Crystals and Molecules", Physical Chemistry Monograph Series, Vol. 29, Academic Press, New York, N.Y., 1973, p 94.
(41) C. K. Johnson, "ORTEP: A Fortran Thermal-Ellipsoid Plotting Program for Crystal Structure Illustrations", Report ORNL-3794, Oak Ridge National Laboratory, Oak Ridge, Tenn., 1965.

Contribution from the School of Chemical Sciences, University of Illinois, Urbana, Illinois 61801, and the Department of Chemistry, University of Colorado, Boulder, Colorado 80309

Preparation and Characterization of Organoiridium Cluster Compounds from the Reaction of Dodecacarbonyltetrairidium with 1,5-Cyclooctadiene. Crystal Structure of $Ir_4(CO)_5(C_8H_{12})_2(C_8H_{10})$

GORDON F. STUNTZ, JOHN R. SHAPLEY,* and CORTLANDT G. PIERPONT*

Received March 23, 1978

The reaction of $Ir_4(CO)_{12}$ with 1,5-cyclooctadiene in refluxing chlorobenzene provides $Ir_4(CO)_5(C_8H_{12})_2(C_8H_{10})$ as the major product together with $Ir_7(CO)_{12}(C_8H_{12})(C_8H_{11})(C_8H_{10})$ in trace amounts. Single-crystal X-ray diffraction has shown $Ir_4(CO)_5(C_8H_{12})_2(C_8H_{10})$ to have a *closo*-Ir_4C_2 pseudooctahedral framework analogous to that of $Co_4(CO)_{10}(C_2Et_2)$. The use of $Me_3NO{\cdot}2H_2O$ as an oxidative decarbonylation reagent allows formation of the derivatives $Ir_4(CO)_{12-2x}(C_8H_{12})_x$ (x = 1–3) under relatively mild conditions. The ^{13}C NMR spectra of these complexes completely define the solution structures. Thermal decomposition of both $Ir_4(CO)_8(C_8H_{12})_2$ and $Ir_4(CO)_6(C_8H_{12})_3$ affords $Ir_4(CO)_7(C_8H_{12})(C_8H_{10})$, which reacts further with 1,5-cyclooctadiene to give $Ir_4(CO)_5(C_8H_{12})_2(C_8H_{10})$. The ^{13}C NMR spectra at several temperatures for $Ir_4(CO)_7(C_8H_{12})(C_8H_{10})$ show two distinct carbonyl scrambling processes, which can be explained by a carbonyl scrambling mechanism related to that previously proposed for $Co_4(CO)_{10}(C_2Et_2)$. The structure inferred for $Ir_4(CO)_7(C_8H_{12})(C_8H_{10})$ from ^{13}C NMR and that determined separately for $Ir_7(CO)_{12}(C_8H_{12})(C_8H_{11})(C_8H_{10})$ by X-ray diffraction suggest a pathway for the transformation of tetrahedral $Ir_4(CO)_{12}$ into pseudooctahedral $Ir_4(CO)_5(C_8H_{12})_2(C_8H_{10})$.

Reactions of iron triad metal carbonyl cluster compounds $M_3(CO)_{12}$ (M = Fe, Ru, Os) and $H_4M_4(CO)_{12}$ (M = Ru, Os) with unsaturated organic substrates have received considerable attention; activation of C–H bonds has proved to be a characteristic feature.[1] Less attention has been devoted to examination of analogous reactions for carbonyl clusters in the cobalt triad. The reactions of $YCCo_3(CO)_9$ (Y = alkyl, aryl, or F) with norbornadiene and 1,3-cyclohexadiene give products characterized as $YCCo_3(CO)_7$(diene); with cyclopentadiene, however, $YCCo_3(CO)_4(C_5H_5)_2$ is isolated.[2a–c] Simple substitution products from the reaction of $YCCo_3(CO)_9$ with trienes,[2c] arenes,[2d] and cyclooctatetraene[3] also have been reported. The reactions of $Rh_4(CO)_{12}$ with 1,5-cyclooctadiene, norbornadiene, 1,4-cyclohexadiene, and 2,3-dimethyl-1,3-butadiene afford hexanuclear products formulated as $Rh_6(CO)_{14}$(diene).[4] Additionally, the compounds $Rh_6(CO)_{12}$(norbornadiene)$_2$ and $Rh_6(CO)_{10}$(norbornadiene)$_3$ have been mentioned.[5] However, treatment of $Co_4(CO)_{12}$ with the above dienes gives dinuclear $Co_2(CO)_4$(diene)$_2$.[4] Compounds formulated as $Co_4(CO)_9(C_7H_8)$, $Co_4(CO)_6(C_7H_8)_2$, and $Rh_4(CO)_8(C_8H_8)$ also have been reported,[4] along with a number of compounds of the general formulation $Co_4(CO)_9$(arene).[6–8] Finally, the reaction of substituted acetylenes with $Co_4(CO)_{12}$ and $Rh_4(CO)_{12}$ gives $M_4(CO)_{10}(C_2R_2)$.[9–12]

In the course of a general survey of the chemistry of $Ir_4(CO)_{12}$, we have isolated a number of cluster compounds from the reaction of $Ir_4(CO)_{12}$ with 1,5-cyclooctadiene. Some of these compounds are simply substitution products, but others are formed as the result of C–H bond scission in the organic ligand. We report here the preparation, characterization, and some interconversions of these new cluster compounds together with the crystal structure of $Ir_4(CO)_5(C_8H_{12})_2(C_8H_{10})$.

Experimental Section

$Ir_4(CO)_{12}$ was prepared by a published method.[13] $Me_3NO{\cdot}2H_2O$ (Aldrich) was used as received. Solvents were obtained commercially and generally used without further purification. 1,5-Cyclooctadiene (Aldrich) was passed over alumina prior to use. Preparative-scale TLC plates were prepared with Merck silica gel G.

Infrared spectra were recorded on a Perkin-Elmer 467 spectrophotometer. ^{13}C NMR spectra were recorded on a JEOL FX-60 spectrometer (15 MHz) with $Cr(acac)_3$ (ca. 0.03 M) added as a relaxation agent. ^1H NMR spectra were recorded on Varian HR-220 (200 MHz), Varian HA-100 (100 MHz), and JEOL FX-60 (60 MHz) spectrometers. Electron impact mass spectra were obtained by Mr. Joe Wrona on a Varian-MAT CH-5 mass spectrometer using an ionizing voltage of 70 eV. Field-desorption mass spectra were determined by Mr. Carter Cook on a Varian 731 mass spectrometer. Microanalyses were performed by the University of Illinois analytical laboratory under the direction of Mr. Joseph Nemeth.

$Ir_4(CO)_5(C_8H_{12})_2(C_8H_{10})$ and $Ir_7(CO)_{12}(C_8H_{12})(C_8H_{11})(C_8H_{10})$. To a refluxing solution of chlorobenzene (50 mL) and 1,5-cyclooctadiene (2 mL) was added solid $Ir_4(CO)_{12}$ (250 mg). The resulting solution was heated at reflux under nitrogen for 18 h. The solvent was then removed at reduced pressure to give a brown oil, and the oil chromatographed on a Florisil column. Elution with pentane generated a small green fraction. Further purification of this fraction by preparative-scale TLC (pentane) led to green $Ir_7(CO)_{12}(C_8H_{12})(C_8H_{11})(C_8H_{10})$ (16 mg, 3.5%) as well as yellow $Ir_4(CO)_8(C_8H_{12})_2$ (2 mg, 0.7%) which was identified on the basis of its mass spectrum. Further elution from the column with pentane–dichloromethane (1:1) gave a dark brown-orange band. This fraction was collected and purified further by preparative-scale TLC (pentane–dichloromethane, 3:1) to give a pink solid (1.5 mg, 0.5%), formulated as $Ir_4(CO)_6(C_8H_{12})_2(C_8H_{10})$ on the basis of mass spectrometry, and brown $Ir_4(CO)_5(C_8H_{12})_2(C_8H_{10})$ (121 mg, 43%). Elution from the column with dichloromethane gave a brown-black band. Purification of this fraction by preparative-scale TLC (pentane–dichloromethane, 1:2)

0020-1669/78/1317-2596$01.00/0